Macalester Journal of Physics and Astronomy

Volume 5
Issue 1 *Spring 2017*

Article 5

May 2017

The Chiral Magnetic Effect in Heavy Ion Collisions From Hydrodynamic Simulations

Elias Lilleskov
Macalester College, Indiana University, elillesk@macalester.edu

Abstract

The quark-gluon plasma created in heavy ion collisions is an exotic state of matter in which many unusual phenomena are manifested. One such phenomenon is the "Chiral-Magnetic Effect" (CME), wherein the powerful magnetic fields generated by colliding ions spin-polarize chiral quarks, causing a net transport effect in the direction of the fields. The CME predicts specific charge-dependent correlation observables, for which experimental evidence was reported, although the evidence is subject to background contamination. Isobaric collision experiments have been planned for 2018 at RHIC, which will study this effect by comparing 96Ru-96Ru and 96Zr-96Zr collisions. The two colliding systems are expected to have nearly identical bulk properties (including background contamination), yet about 10% difference in their magnetic fields due to different nuclear charges. This provides a unique opportunity to disentangle the CME observable and background effects. By simulating this effect using anomalous hydrodynamic simulations, we make a quantitative prediction for the CME-induced signal for several centralities in each of these two colliding systems. Our results suggest a significant enough difference in the signal to be experimentally detected- on the order of 15-20%.

The Chiral Magnetic Effect in Heavy Ion Collisions From Hydrodynamic Simulations

Cover Page Footnote
Many thanks to my research group at the Center for Exploration of Energy and Matter (CEEM) at Indiana University led by Professor Jinfeng Liao, consisting of Shuzhe Shi and Dr Yin Jiang. Also thanks to those the Indiana University REU program for giving me the opportunity to conduct this research, especially Dr John Carini and Dr Garfield Warren, and the NSF who funded the program.

The Chiral Magnetic Effect in Heavy Ion Collisions From Hydrodynamic Simulations

Elias Lilleskov

1 Introduction

1.1 Heavy Ion Collisions

Heavy ion collisions are collisions that occur when two beams of ions − such as lead, gold, ruthenium or zirconium − are accelerated at one another. At really high energies, such as in the Relativistic Heavy Ion Collider (RHIC) which has a C.O.M. energy of 200 GeV[2] − a "quark-gluon plasma" is generated. This is an exotic state of matter where quarks are no longer bound up in protons or neutrons. This is because of the process of deconfinement, wherein the interaction strength of the strong nuclear force approaches zero at high energies. Instead, the quarks and gluons freely interact in a low-viscousity superfluid. The particles will typically collide in an almond-shaped region (see the region of overlap in figure 1). As the fluid flows, it will tend to move more quickly in the regions with lower pressure gradients (the "sides" of the almond) and flow more slowly in regions with higher pressure gradients (the "points" of the almond). This will lead to an "elliptic flow", which lets experimentalists predict the orientation of the collision. [3].

The shape/size of the overlap region is determined by the "impact parameter" (b) which describes the distance between the centers of the colliding nuclei. Small impact parameter collisions are described as being central, while large impact parameter collisions are described as being peripheral. This leads us to how we can determine experimentally determine how central a collision is. In principle, more central collisions will have a larger overlap region between the nuclei, and so will have more "participants" and fewer "spectators" (particles which interact and those that do not). Mulitplicity measures the total number of particles detected in a collision, larger for more central collisions. Conversely, spectator energy will be larger for more peripheral collisions. Upon evaluating all the events that occur in a collider, they are ranked from largest to smallest predicted centrality according to the aforementioned measurements and other related quantities. The events are then binned from 0-100%, with 0% being the most central collision and 100% being the

most peripheral. Thus "larger" values of centrality describe more peripheral collisions [4]. For most collisions, the relationship between centrality and impact parameter is very close to cent $= \pi b^2/\sigma$, where σ is the interaction cross-section of the two nuclei, although this breaks down a bit for the most peripheral collisions [5]. Luckily, highly peripheral collisions are less important for our purposes, and so we can safely ignore this discrepancy.

1.2 P- and CP- symmetries

In order to understand the chiral magnetic effect, we must briefly review the concept of $C-$ and $CP-$ symmetries. In general, symmetries are one of the most important aspects of nature we study as physicists. It has in fact been said by Nobel laureate Phillip Warren Anderson that "it is only slightly overstating the case to say that physics is the study of symmetry."[1] Two of the most important symmetries in physics are parity and charge. Parity (P) symmetry is symmetry on inversion of spatial coordinates and charge (C) symmetry is symmetry on swapping positive and negative charges. Upon transformation through these symmetries, the vast majority of quantities in physics are either even or odd, depending on whether they retain their sign or if it is swapped. Mathematical objects which have no dependence on charge, such as mass or momentum, will be C-even. Some examples of mathematical objects that are C-odd should be intuitevely obvious; examples include magnetic fields, electric fields and current. In the case of parity transformations, it is slightly less obvious. P-even objects include vectors and scalars - things that cannot be written as the cross product of other quantities. Examples of P-even vectors include electric fields, velocity and current, examples of P-even scalars include charge, mass and electric potential. On the other hand we have P-odd quantities, which include pseudovectors and pseudoscalars. Examples of pseudovectors include magnetic fields and angular momentum vectors, and an example of a pseudoscalar is helicity, the dot product of momentum (P-even) and angular momentum (P-odd).

By convention, this is typically discussed in terms of C- and CP-symmetry. A CP

transformation is simply a simultaneous charge and parity transformation − we switch the sign of all the charges and invert all spatial coordinates. If something is C-even and P-odd or C-odd and P-even it will be CP-odd, and if some quantity is either odd for both C and P or even for both C and P it will be CP-even.

1.3 CME

One of the most interesting aspects of physics is the way in which microscopic laws can cause emergent behavior at larger scales. One example of this is Ohm's law:

$$\vec{J} = \sigma \vec{E}$$

In Ohm's law, the current of electric charge is determined by the conductivity of a material, and the strength of the electric field. It is important to not here that both the current and the electric field are P-odd and CP-odd, and the conductivity σ must therefore be P-even and CP-even. Ohm's law emerges from microscopic electromagnetic interactions within materials. It turns out that more exotic processes can show emergent behavior as well. One such process is the chiral-magnetic effect (or CME). The CME can be described by the following analog of Ohm's law[2]:

$$\vec{J} = C_A \mu_A \vec{B}$$

Here, C_A and μ_A are scalars. If we recall that $\vec{J}$ is P-even and CP-odd and that $\vec{B}$ is P-odd and CP-even, we realize that $C_A \mu_A$ is P-odd and CP-odd, and so is not a normal material property. It turns out that C_A is a constant determined by the specifics of quantum-chromodynamics (QCD), and it is equal to $\frac{N_c e}{2\pi^2}$ [2], where N_c is the number of colors in QCD, which is 3, and so C_A is a P- and CP-even scalar. We must then conclude that μ_A is a P-odd and CP-odd pseudoscalar.

μ_A is in fact the "chiral chemical potential"- a chemical potential which describes the imbalance of left- and right- handed quarks. This imbalance arises because the mass of the light quarks is much less than the energy of the QGP, and so the particles are well described

by the low-mass limit in which they are all chiral − meaning their helicity is fixed. Right-handed particles would be particles whose spin vectors (technically spin *pseudo*vectors) and linear momentum vectors will be aligned, and for left-handed particles they will be anti-aligned. Under typical conditions one might expect an equal number of right- and left-handed quarks. However, topological fluctuations in QCD can give rise to temporary, local imbalances in the number of right- and left-handed quarks. It has also been proposed that P- and CP-violations in QCD which have not been seen at low energies may in fact emerge at higher energies. Both of these causes arise from very fundamental physics [2].

We can imagine the chiral magnetic effect in a simple representative picture. Say there are more right- than left-handed quarks, and that they are all positively charged. A powerful magnetic field then polarizes the quarks, aligning their spins with the magnetic field. Since their linear momenta are aligned (for right-handed quarks) or anti-aligned (for left-handed) with their spin, they will move in the direction of the magnetic field if they are right handed, or against if they are left handed. This creates a current parallel or anti-parallel with the magnetic field. Although we assumed the quarks were positively charged, this holds just as well if they are negatively charged, since they move in the opposite direction and thus move the net charge in the same manner.

In light of this, upcoming experiments at RHIC intend to collide $Ru^9$6-$Ru^9$6 and $Zr^9$6-$Zr^9$6, which should be very similar collisions, except that Ruthenium has slightly more protons. This means there will be a stronger magnetic field, and presumably a stronger CME effect. This should provide a sensitive test of CME, as it can rule out other possible effects that might produce similar signals. This paper attempts to predict the difference in the signal for each collision type.

2 Methodology

2.1 Magnetic Field Strength

We can use an "optical" model to get an estimate of the magnetic field strength during the collision. An optical model imagines the nuclei as "balls" of charge, whose charge density follows the Woods Saxon distribution:

$$\rho(r) = \frac{\rho_0}{1 + e^{(r-R_0)/a}}$$

. Parameters for Ruthenium and Zirconium were taken from reference [6]. We then find the electric fields for each particle using Gauss' law, and transform them to the moving frame using [7]:

$$\vec{\mathbf{B}} = -\frac{\gamma}{c^2}(\vec{\mathbf{v}} \times \vec{\mathbf{E}})$$

. Since the nuclei are so length contracted, we can treat the collision as 2-dimensional for most purposes. Assuming the particles are moving along the z axis, we find that the electric field at rest from a single nucleus has magnitude:

$$|E| = \frac{\alpha}{3e} \frac{1}{4\pi(x^2 + y^2 + z^2)} \int_0^{\sqrt{x^2+y^2+z^2}} \rho[r]dr$$

. with all coordinates measured from the center of the nucleus, and α being the fine structure constant. Then the magnetic field in some planar x-y slice in the lab frame is then:

$$\vec{B}[x, y] = \pm\sqrt{\gamma^2 - 1}\frac{\alpha}{3e} \frac{1}{4\pi(x^2 + y^2 + (\gamma z_0)^2)} \int_0^{\sqrt{x^2+y^2+(\gamma z_0)^2}} \rho[r]dr \left(\frac{|\vec{y}|\hat{x} - |\vec{x}|\hat{y}}{\sqrt{x^2 + y^2 + (\gamma z_0)^2}} \right)$$

. Here z_0 is the (lab-frame) distance of the center of the nucleus out of the plane in consideration. The $\pm$ is $+$ if the nucleus is travelling out of the plane, and $-$ if it is travelling into the plane. The final magnetic field for a particular z_0 is then just

$$\vec{B}(x, y) = \vec{B}_{out}(x + b/2, y) + \vec{B}_{in}(x - b/2, y)$$

Here b is the impact parameter, and we have assumed that the origin is exactly between them, with the x-z plane intersecting their centers. This will result in a magnetic field which is roughly constant in magnitude and direction in the bulk of the overlap region (see figure 1). We can then convert this dependence on b to a dependence on centrality using a formula found from modelling the collision: $b = 1.24 * \text{cent}^{1/2}$. What we are interested in is the magnetic field strength in the center of the overlap region between the nuclei, since we will assume that this is the value of the magnetic field strength throughout the plasma.

To be more robust, we can compare the strength of the magnetic field at the center of the collision to that found in Monte Carlo simulations of collisions done by a different research group (see figure 2) [8]. The values are similar, but not identical. The difference can likely be accounted for by the fact that, because the Monte Carlo simulation deals with discrete particles rather than a smooth distribution of particles, small asymmetries may arise and the magnetic field wil not always point perpendicular to the x-z plane. [8] Ultimately, the Monte Carlo generated values are likely to be more accurate, as it is a more detailed calculation.

2.2 Hydrodynamic Simulation

Because the quark-gluon plasma has the properties of a superfluid, it's behavior is well-approximated by hydrodynamic simulations. Indeed, hydrodynamic simulations have captured many of the experimentally-determined effects in the QGP. The anomolous hydrodynamics simulations discussed in reference [9] add on anomolous hydrodynamic effects that simulate the CME. The additional equations solved are:

$$\partial_\mu J^\mu = \partial_\mu (n u^\mu + Q_f C_A \mu_A B^\mu) = 0$$

$$\partial_\mu J^\mu_A = \partial_\mu (n_A u^\mu + Q_f C_A \mu_V B^\mu) = -Q_f^2 e C_A E_\mu B^\mu$$

. These equations are solved for each quark flavor. Q_f is the charge for each flavor. C_A is just the the constant given above. E_μ and B_μ are covariant electromagnetic fields. μ_A and

μ_V are the axial and vector chemical potentials, determined from their respective number densities using results from lattice QCD. n is the number density of the particular flavor of quark. u^μ is the flow field, taken from the background hydrodynamic solutions. Ultimately, the parameters which are not fixed and which have the most bearing on the CME are n_A, the axial quark density (the difference between the right- and left-handed quark densities), and the magnetic fields. More specifically, we input $N_A = n_a/s$, where s is the entropy density. For more details on the simulation, see reference [9]. The magnetic fields are assumed here to be uniform in magnitude and direction, with a fixed lifetime determined by $B = B_0/[1 + (\tau/\tau_B)^2]$, where τ_B is 0.6 fm/c for this paper.

So in a given collision, we choose the centrality (which fixes the magnetic field strength) and input several values for N_A, as there is a great deal of theoretical uncertainty for this number, and in fact it likely varies from collision to collision, as it is induced by topological fluctuations in QCD. We first used N_A=0, 0.05, 0.10 and 0.15 for centralities of 10-20%, 20-30%, 30-40%, 40-50%, 50-60% and 60-70%. We then used centrality dependent values for N_A, because in fact $N_A \propto S^{-1/3}$ [9], and $S \propto n_{part}$, the total number of participants in the collision. Ultimately we have that $N_A = k/N_{part}^{1/3}$, where $k = 0.48$ was chosen for this simulation, but can be freely adjusted within reasonable parameters. The values of N_{part} are 84.07, 56.33, 38.53, 27.35, 20.19, 15.28 for the above centralities, respectively.

2.3 Detection Simulation

In this simulation, after the system evolves and the temperature cools, a "freeze-out" is imposed. As the actual phase-transition is poorly understood, this is done ad-hoc, translating the fluid that was treated as continuous to a set of discrete particles. After hadron freeze-out occurs, the particles then decay to their probable products, and are "detected" with various momenta and angles. An angular and momentum distribution function of the form $f[\phi] = v_0 + 2a_1 \sin[\phi] + 2v_1 \cos[\phi] + 2a_2 \sin[2\phi] + 2v_2 \cos[2\phi] + \ldots$ is found for each decay product, and then integrated across the momentum range RHIC is

sensitive to, giving integrated values for a_1, v_1, etc. For detecting the CME, the most important parameter is a_1, since it represents effects that are odd on reflection across the "x"-axis. A positive a_1 indicates more particles were deposited in the direction of the magnetic field, whereas a negative a_1 indicates more particles were deposited in the opposite direction. For our purposes, we are chiefly concerned with a_1 for π^+ and π^- mesons, since these will tell us about the charge seperation induced by the CME, and represent a significant percentage of the decay products.

3 Results and Discussion

We can see a variety of effects in examining a_1. Looking at figure 3, it is apparent that, for fixed centrality, the dependence of a_1 on N_A is quite linear. We can also see that the signal is slightly stronger from Ru than from Zr, because Ru has a stronger magnetic field. We can also look at what happens across different centralities for a fixed N_A, as in figure 4. Here we see that a_1 is certainly centrality dependent, but does not have a neat linear relationship. Instead it levels off as the magnetic field strength peaks for the more peripheral collisions plotted.

Recall however that the primary mechanism of generating N_A − the topological fluctuation − does not prefer more right- than left- handed quarks being generated or vice versa, and so if events are averaged to get a stronger signal, the effects will vanish, because for every positive N_A event there will be equally many negative N_A events on average, cancelling the net signal. The so-called H-correlator may be an observable that can be used to determine the magnitude of CME effects in experiment. In principle the H-correlator should go as a_1^2. The H-correlator is meant to cancel out background and other irrelevant effects, although there is some question as to what extent this will work in practice[10].

Operating on the assumption that H a_1^2, we can find values for the H-correlator*Npart for Zr and Ru (see figures 5 and 6). We can also find the ratio between them (figure 7). For these calculations of H, we use the centrality dependent value of N_A as described above.

4 Conclusion

In this paper we have examined the chiral magnetic effect and its ability to search for anomolous physics. The suggestion from this work is that the signal will be detectable in upcoming experiments at RHIC, with a ratio between the values of H for the two colliding systems around 1.2 (see figure 7). Assuming the background is not too significant, this should allow us to confirm the presence of anomolous physics to a good deal of accuracy. Additional work by my research group has added complexity to the hydrodynamic simulations, allowing for more accurate predictions [12, 13].

5 References

[1] Anderson, P. W. 1972. http://robotics.cs.tamu.edu/dshell/cs689/papers/anderson72more_is_different.pdf

[2] Liao, Jinfeng. 2015. https://arxiv.org/pdf/1401.2500.pdf

[3] Jacak, Barbara V. and Mller, Berndt. 2012. http://rhig.physics.yale.edu/Summer2014/Jacak_Mueller.pdf

[4] Toia, Alberica. 2013. http://cerncourier.com/cws/article/cern/53089

[5] Broniowski, Wojciech and Florkowski, Wojciech. 2001. https://arxiv.org/pdf/nucl-th/0110020.pdf

[6] Nuclear charge-density-distribution parameters from elastic electron scattering; Atomic Data and Nuclear Data Tables Volume 36, Issue 3, May 1987, Pages 495-536

[7] Griffiths, D.J. Introduction to electrodynamics, 3ed.

[8] Deng, Wei Tian et. al. 2016. https://arxiv.org/pdf/1607.04697.pdf

[9] Yin, Yi and Liao, Jinfeng. 2016. https://arxiv.org/pdf/1504.06906v2.pdf

[10] Kharzeev, D.E. et al. 2016. https://arxiv.org/pdf/1511.04050.pdf

[11] Wang, Gang. 2016. https://indico.cern.ch/event/403913/contributions/2142036/attachments/1300204/1940735/SQM_GangWang_2016.pdf

[12] Jiang, Yin et al. 2016. https://arxiv.org/pdf/1611.04586.pdf

[13] Shi, Shuzhe et al. 2017https://arxiv.org/pdf/1704.05531.pdf

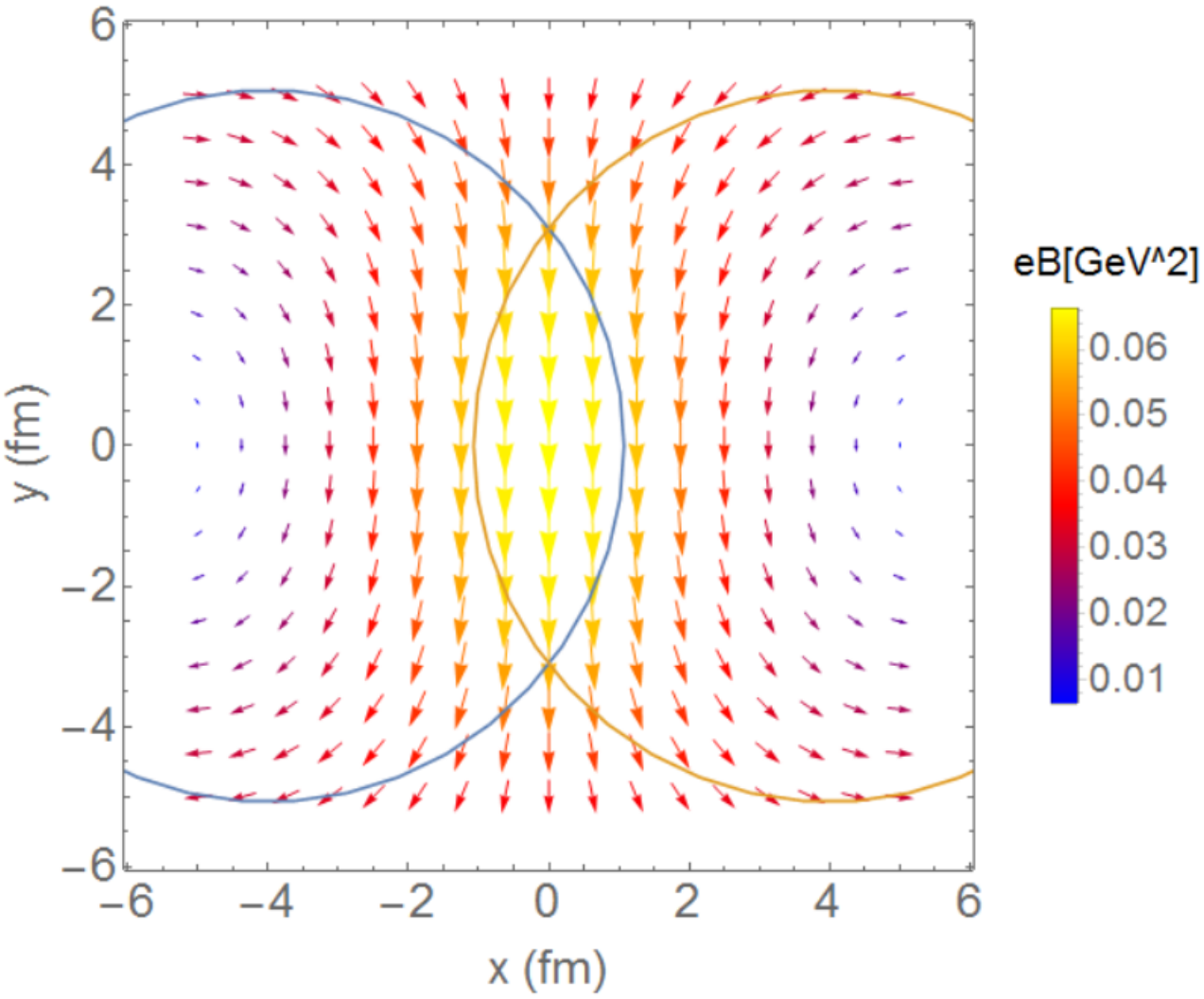

Figure 1 Optical model of magnetic fields for Zr^{96}-Zr^{96} collision, with $z_0 = 0$, $b = 8$ fermi. The blue and orange lines represent the characteristic nuclear radii (R_0 in the Woods-Saxon distribution). The QGP will primarily be created within the almond-shaped overlap region, and one can see that the magnetic field strength is maximized in this region, as well as that it is roughly constant and faces downward.

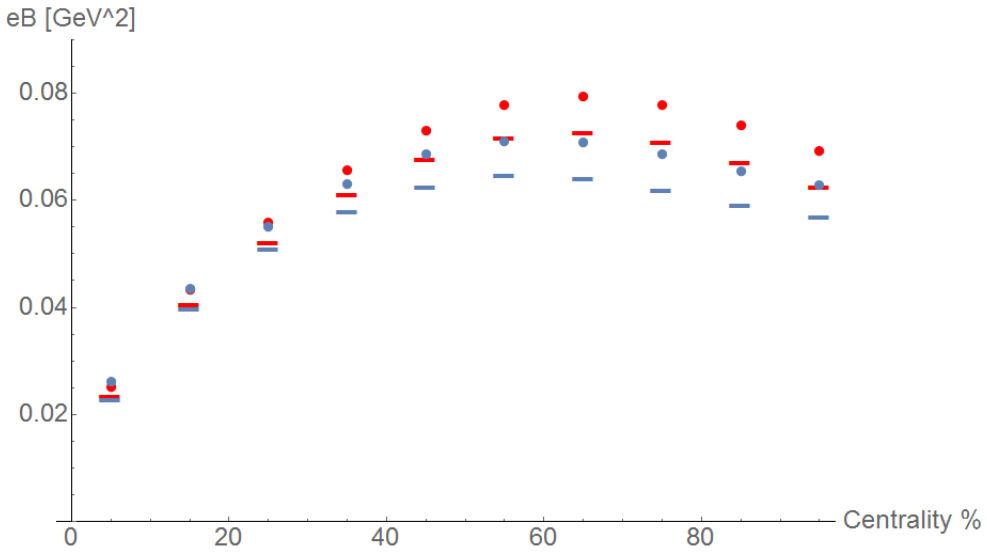

Figure 2 Red indicates magnetic field strength from the optical model, whereas blue is from the Monte Carlo simulations in reference [8]. The dots represent Ruthenium, whereas the lines are for Zirconium. Notice that in both models, the Ruthenium has stronger magnetic fields. Also note that the two models are more similar for smaller centralities.

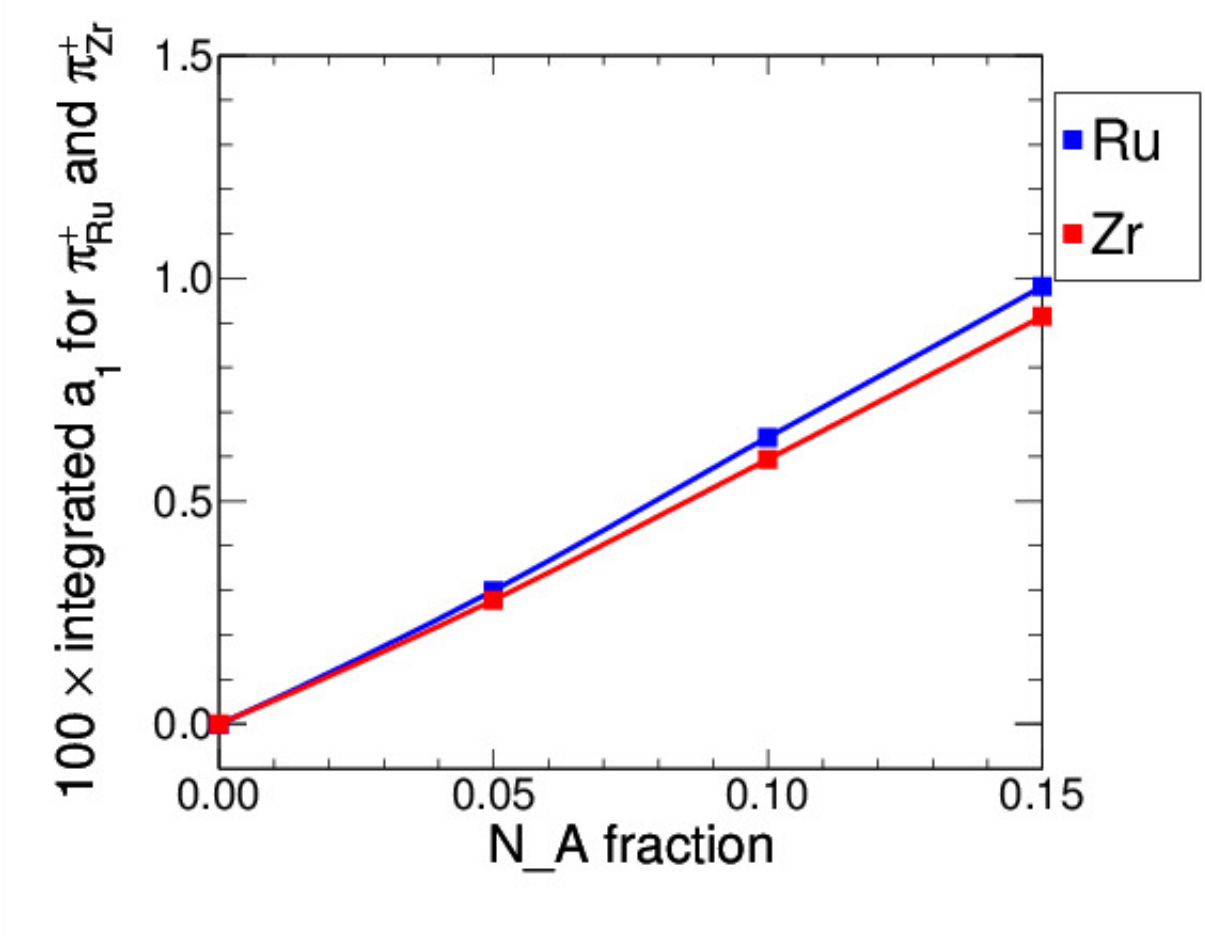

Figure 3 Here we have 100*a_1 for π^+ particles generated in Ru and Zr collisions plotted versus N_A. Note the very linear dependence of a_1 on N_A. Magnetic field strengths here are from the Monte Carlo simulations for 20-30% centrality.

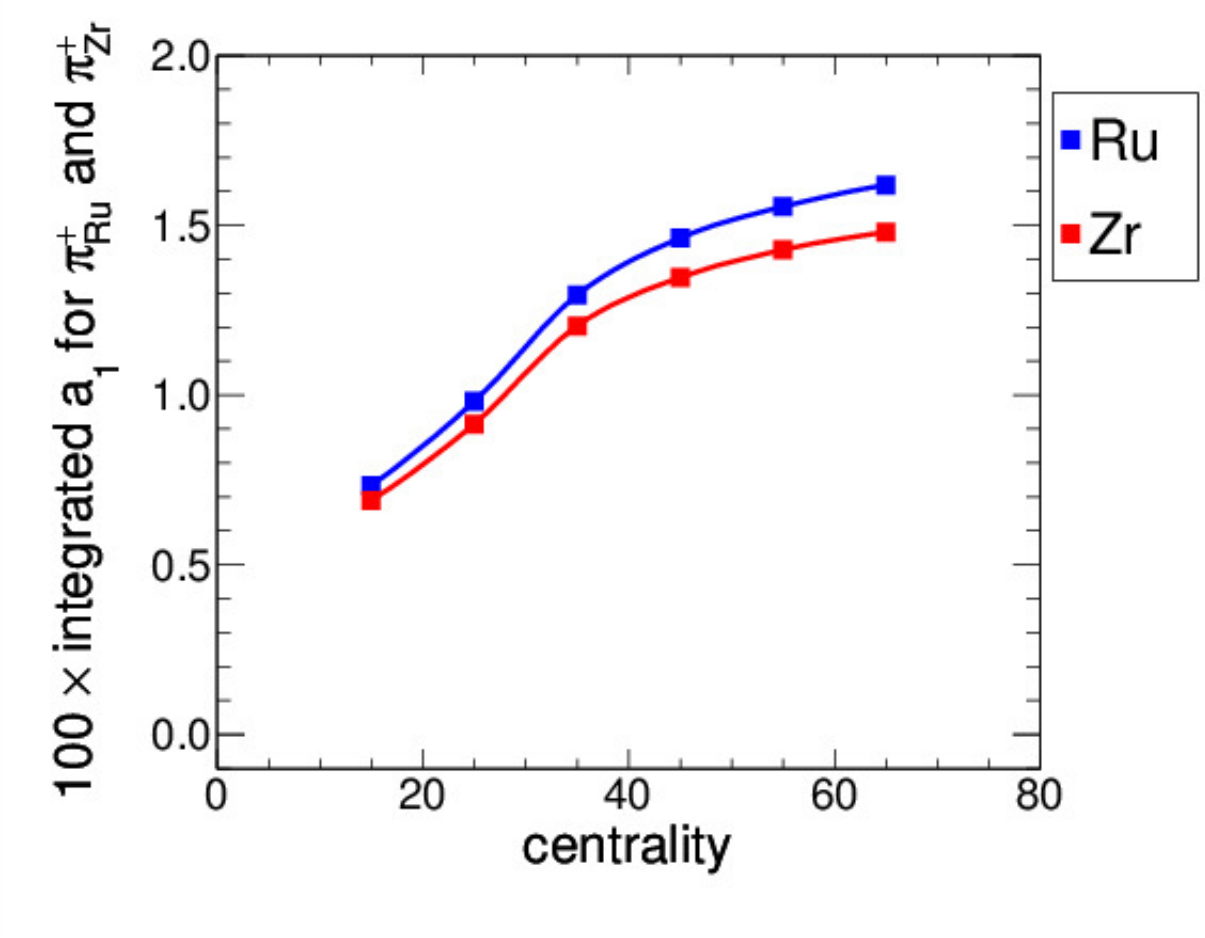

Figure 4 Here we have 100*a_1 for π^+ particles generated in Ru and Zr collisions plotted versus centrality, with N_A fixed at 0.15. Magnetic field strengths here are from the Monte Carlo simulations for. Note that a_1 is again larger for Ruthenium than Zirconium, this time across centralities. Also note that a_1 increases with increasing centrality, but begins to level off as we approach 60-70% centrality, which is around the peak magnetic field strength.

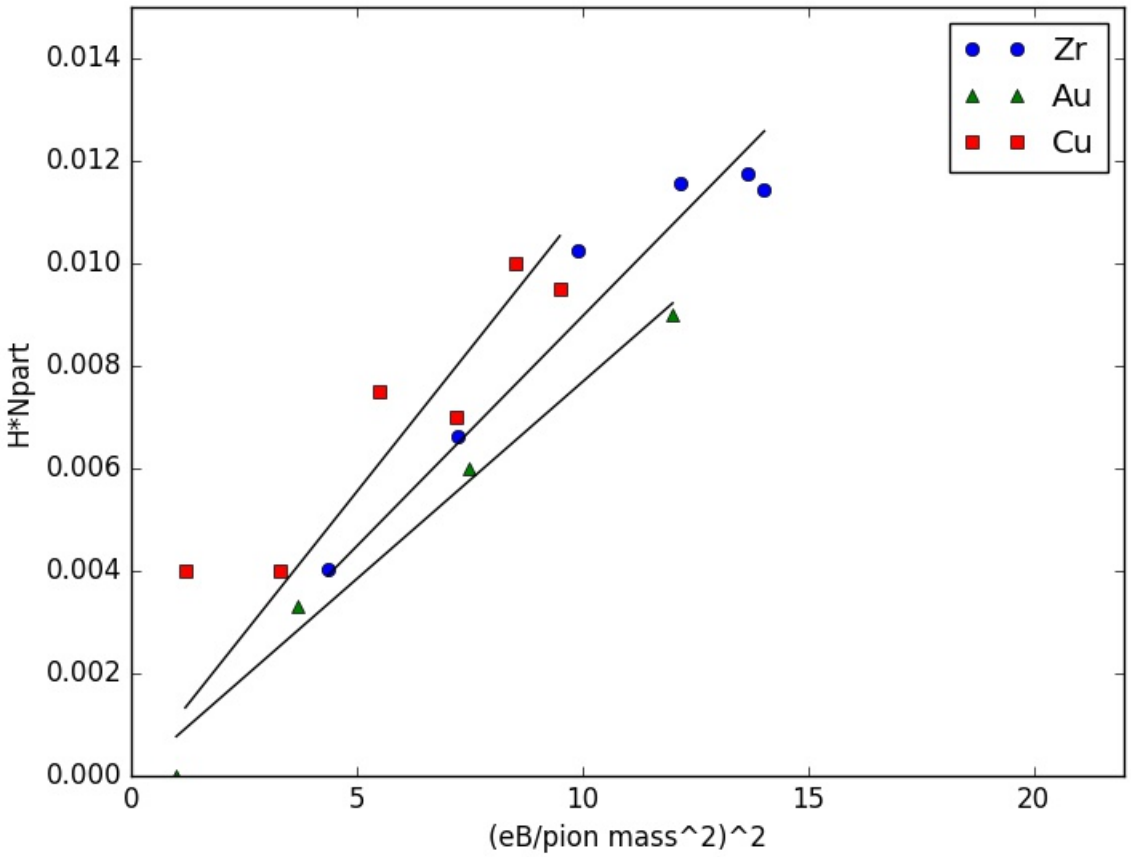

Figure 5 Here we have H*Npart for Zirconium as a function of $(eB/m_\pi^2)^2$. This is plotted against data from [11] for Au and Cu collisions. The data is fairly linear, and the points for Zirconium lie between those for Au and Cu, as other theoretical considerations predict. The magnetic fields from Monte Carlo simulations are used here.

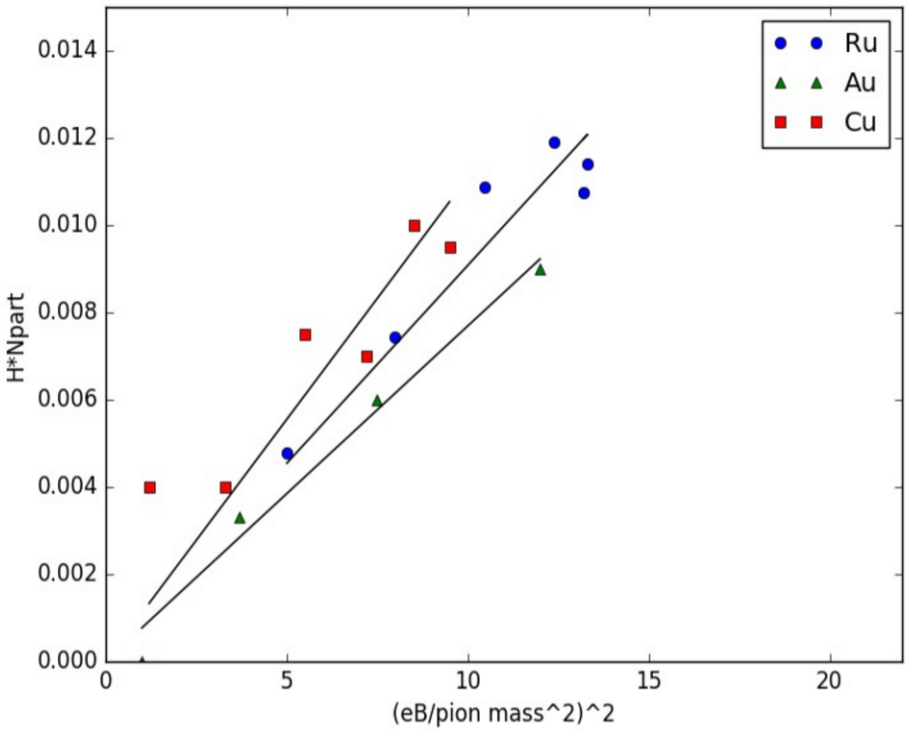

Figure 6 Here we have H*Npart for Ruthenium as a function of $(eB/m_\pi^2)^2$. This is plotted against data from [11] for Au and Cu collisions. The data is fairly linear, and the points for Ruthenium lie between those for Au and Cu, as other theoretical considerations predict. The magnetic fields from Monte Carlo simulations are used here.

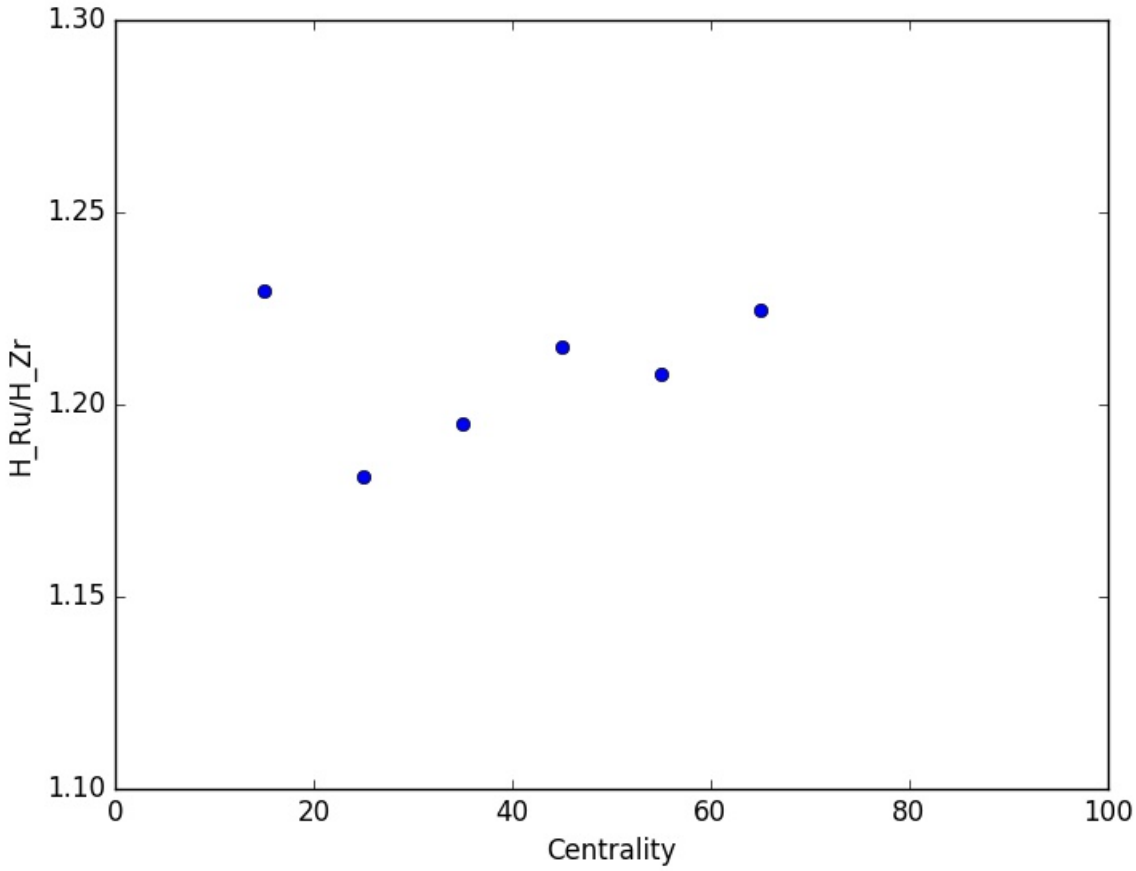

Figure 7 Ratio of H for Ruthenium and Zirconium. The source of the variation across centrality is unclear. Magnetic fields from Monte Carlo simulation.